Journal of Power Sources 231 (2013) 122–133

Contents lists available at SciVerse ScienceDirect

Journal of Power Sources

journal homepage: www.elsevier.com/locate/jpowsour

Electrooxidation of ethanol on Pt-based and Pd-based catalysts in alkaline electrolyte under fuel cell relevant reaction and transport conditions

S. Sun, Z. Jusys, R.J. Behm*

Institute of Surface Chemistry and Catalysis, Ulm University, D-89069 Ulm, Germany

HIGHLIGHTS

- Ethanol electrooxidation in alkaline solution was studied under fuel cell relevant conditions.
- Pt/C, PtRu black, Pd/C and Pd/CeO_2/C catalysts were used.
- Monometallic catalysts show better activities at high temperature and potential.
- Addition of oxophilic components is beneficial only for lower potentials.
- Effective activation energies are derived under steady-state conditions.

ARTICLE INFO

Article history:
Received 14 June 2012
Received in revised form
14 December 2012
Accepted 20 December 2012
Available online 5 January 2013

Keywords:
Ethanol electrooxidation
Alkaline solution
Elevated temperatures
Apparent activation energy
Pt-based catalysts
Pd-based catalysts

ABSTRACT

Aiming at a detailed kinetic understanding under fuel cell relevant, but nevertheless well-defined reaction and transport conditions, the electrooxidation of ethanol on Pt-based (Pt/C, PtRu black) and Pd-based (Pd/C, Pd/CeO_2/C) catalysts in alkaline solution was investigated at temperatures up to 100 °C and at controlled electrolyte flow in a high temperature/high pressure thin-layer flow cell. Most important, the data reveal drastic effects of the reaction temperature. The apparent activation energies for ethanol oxidation on the different catalysts were determined and found to vary significantly with potential and the catalyst used. The addition of Ru to Pt and CeO_2 to Pd/C improves the tolerance toward catalyst poisoning at low potentials, while for higher potentials and especially at higher temperatures the activity of the monometallic catalysts is higher. For reaction at 0.5 V and 80 °C, the Pd/C catalyst exhibits the highest activity, both in terms of metal mass specific and active surface area normalized rates; the addition of an oxophilic component is beneficial only for lower potentials. Overall, the results illustrate the need for model studies under close to realistic reaction conditions for the understanding of reactions in fuel cells.

1. Introduction

The electrooxidation of ethanol has attracted significant interest, both from fundamental reasons, as a model reaction for the electrooxidation of small organic molecules, and because of its potential application in direct ethanol fuel cells [1–6]. For reaction in acidic electrolyte, where most of the studies focused on, it was found that the reaction is kinetically hindered and requires a significant overpotential. Furthermore, efficient catalysis requires expensive noble metal catalysts [7,8]. In acidic medium, platinum is often considered to be the best monometallic catalyst for oxidation of hydrocarbon molecules with its characteristic ability for catalytic C–H bond cleavage, whereas CO_{ad} oxidation on Pt electrodes requires a significant overpotential [5,9]. This is different for reaction in alkaline electrolyte, where overpotentials were found to be significantly lower and where inexpensive transition metal electrodes such as Ni and/or Ru were found to be highly active [10]. Recently, the interest in alkaline ethanol oxidation has been raised considerably by new developments in alkaline anion exchange membranes, which make alkaline ethanol oxidation fuel cells more feasible [11–14], and much of the research was addressed to transition metal electrodes, such as Ni, Au, Ag, Cu, Ru, Zn (also their combination with Pd or Pt) [10,15].

In the present paper, we report results of a comparative study on the EOR kinetics on three different carbon supported catalysts

* Corresponding author. Tel.: +49 731 50 25451; fax: +49 731 50 25452.
E-mail address: juergen.behm@uni-ulm.de (R.J. Behm).

0378-7753/$ – see front matter © 2012 Elsevier B.V. All rights reserved.
http://dx.doi.org/10.1016/j.jpowsour.2012.12.091

(Pt/C, Pd/C and Pd/CeO_2/C) and an unsupported PtRu catalyst (PtRu black). Most important and different from earlier studies, the measurements were performed on structurally well-defined electrodes and at well-defined transport conditions, but under fuel cell relevant reaction conditions, at elevated temperatures, up to 100 °C, and pressure (3 bar overpressure) and under continuous controlled electrolyte transport, which allows direct comparison of the measured reaction kinetics with the reaction in a fuel cell.

Previous studies on the ethanol oxidation reaction (EOR) in alkaline solution on different types of Pt-based or Pd-based electrodes, performed mostly under strongly idealized reaction conditions or as less well-defined fuel cell measurements, had come to the following conclusions: For the EOR in alkaline electrolyte on different types of Pt-based electrodes/catalysts (single crystalline and polycrystalline (pc) platinum and platinum alloys, carbon supported platinum and platinum alloy catalysts), previous studies [16–22] revealed lower overpotentials for the removal of electrode poisoning species such as CO_{ad} than in acidic electrolyte, due to the higher concentration of hydroxyl species [23]. Lai et al. [19,21] reported a considerable enhancement of the EOR activity on a pc platinum electrode in 0.1 M NaOH solution ethanol as well as a negative shift of about 100 mV in the onset potential (~50 mV in peak potential) compared to that in 0.1 M $HClO_4$ solution for similar ethanol concentration (0.5 M). Jiang et al. [20] determined an increase of the EOR current density on a Pt/C catalyst by factors of 4 (at 0.5 V vs. RHE) or 5 (at 0.6 V vs. RHE) in 0.1 M NaOH solution compared with those in 0.5 M H_2SO_4 solution (both cases 0.01 M ethanol) at room temperature, connected with a cathodic shift of the onset potential by about 80 mV. The addition of Sn to a Pt/C (PtSn/C) catalyst showed a negligible improvement in the EOR kinetics compared with that of a Pt/C catalyst in alkaline solution, in contrast to findings in acidic solution, where bimetallic PtSn catalysts are considered as most active catalysts [7,8,24–26]. A similarly small difference was observed also for a Pt_2Ru_3 catalyst, compared to a Pt/C catalyst, in the MOR kinetics in alkaline solution [27]. Also the product distribution in the EOR was much more favorable in alkaline than in acidic electrolyte. Rao et al. [17], who quantitatively determined the product distribution in a direct ethanol oxidation fuel cell by online mass spectrometry measurements, reported CO_2 current efficiencies in the order of 55% at a potential of 0.8 V vs. RHE on a Pt electrode (60 °C, 0.1 M EtOH in 0.2 M KOH), which is significantly higher than the CO_2 current efficiencies obtained in acidic media under similar conditions [17,28].

Palladium is known as a poor electrocatalyst for alcohol oxidation in acidic medium, but shows a remarkable EOR activity in alkaline environment [22,29–38]. Zheng et al. [39] investigated the activity of Pd catalysts, employing different types of support, and compared it with that of a Pt/C catalyst (in 1 M KOH + 1 M EtOH). They found that a multiwall carbon nanotube (MWCNT) supported Pd catalyst exhibited a higher activity, by a factor of 3, than the Pt/C catalyst. In order to improve the electrocatalytic activity and stability, oxide supports such as CeO_2 were added to the Pd/C catalyst [40], which increased the EOR activity in 1 M KOH containing 1 M ethanol compared to that of the pure Pd/C catalyst [33,40].

In the following, we will first briefly describe the setup used for these measurements and the experimental procedures. Next, we will present and discuss results on pre-adsorbed CO oxidation (Section 3.1), followed by potentiodynamic (Section 3.2) and potentiostatic (Section 3.3) measurements in 0.5 M NaOH. We will compare the mass specific and active surface area specific activities of the respective electrodes in the temperature range between 23 °C and 80 or 100 °C, respectively, at different potentials (Section 3.4). Apparent activation energies for ethanol oxidation reaction in alkaline solution on the Pt- and Pd-based catalysts were derived under similar reaction condition and discussed in the last part (Section 3.5).

2. Experimental

2.1. High temperature/high pressure flow cell setup

The high temperature/high pressure thin-layer channel flow cell [41] with well-defined mass transport characteristics used in this study is shown in Fig. 1. A Pt wire located in a separate compartment served as a counter electrode, an external saturated calomel electrode (SCE) kept at ambient temperature was used as a reference electrode (for details see Ref. [41]). All potentials, however, are quoted against those of a reversible hydrogen electrode (RHE) at the respective reaction temperature, which were determined in separate hydrogen evolution/oxidation experiments in H_2-saturated supporting electrolyte at each temperature [41]. The cell was located in an air thermostat and connected to a pressure-resistant syringe pump (Harward Apparatus 11plus), which controlled the electrolyte flow rate, and the pressurized glass bottles for electrolyte supply. The latter were thermostated separately in thermostats (Lauda E200). Connections were made from PEEK capillaries. The electrolyte was pressurized after purging with high purity N_2.

2.2. Electrode preparation

The circular thin-film catalyst electrodes (diameter ca. 5 mm, accessible geometric surface area 0.2 cm^2) were prepared from commercial Pt/C (20 wt.% Pt, E-TEK Inc.); Pd/C (5 wt.% Pd, Degussa.); Pd/CeO_2/C (10 wt.% Pd, Hypermec Acta.); PtRu black (atomic ratio Pt:Ru = 1:1, Johnson Matthey) catalysts via the procedure described in Ref. [42], by pipetting and drying 20 μl of an ultrasonically re-dispersed aqueous catalyst suspension, and then 20 μl of aqueous Nafion solution, in the center of the mirror-polished rectangular glassy carbon plate (Sigradur G from Hochtemperatur Werkstoffe GmbH, 30 mm × 20 mm × 6 mm). This plate was mounted on the flow cell body (machined from PEEK) and pressed against a gasket with a pre-cut channel (for details see Ref. [41]). The resulting metal loadings were 10 $\mu g_{Pt}\,cm^{-2}$ for Pt/C, 40 $\mu g_{Pd}\,cm^{-2}$ for Pd/C, 40 $\mu g_{Pd}\,cm^{-2}$ for Pd/CeO_2/C, and 100 $\mu g_{(PtRu)}\,cm^{-2}$ for PtRu black. The corresponding mass specific

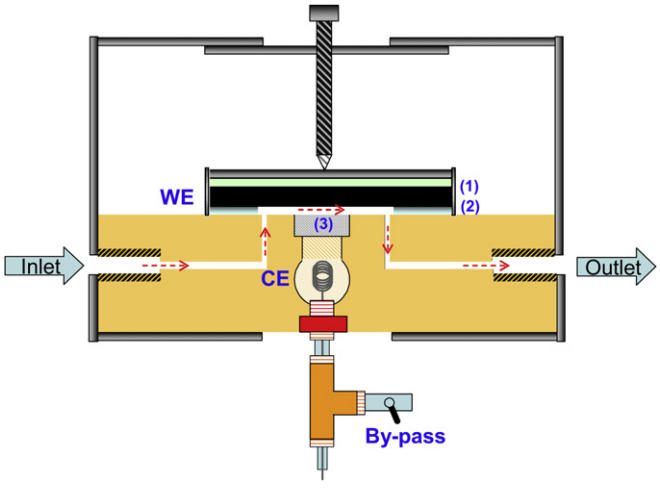

Fig. 1. Schematic drawing of the electrochemical high temperature/high pressure (HT/Hp) thin-layer channel flow cell: (1) working electrode (WE), (2) gasket, (3) porous glass frit. The reference electrode (saturated calomel electrode, SCE) is connected at the inlet of the cell via a Luggin capillary. A by-pass for the electrolyte helps to remove the gas bubbles formed at the counter electrode. The electrolyte flow is depicted by the arrows (from inlet to outlet).

currents (Section 3.3) were then obtained by normalizing the Faradaic currents to the respective metal component mass.

Prior to each measurement, the cell was carefully flushed with the supporting electrolyte, then the thin-film electrode was cycled in the potential range between 0.06 and 1.16 V for the Pt/C and Pd/C catalysts, from 0.06 to 0.8 V for the PtRu black catalyst and from 0.1 to 1.2 V for the $Pd/CeO_2/C$ catalyst (all at 100 mV s^{-1} scan rate), until the cyclic voltammogram of a clean electrode was reproduced.

The electrochemically active surface areas were determined separately from pre-adsorbed saturated CO adlayer oxidation (CO_{ad} stripping) in a three-electrode beaker cell at room temperature (see Section 3.1) after CO adsorption for 5 min and removal of the CO residues from the electrolyte by purging in N_2 saturated electrolyte for about 30 min [42].

The supporting electrolyte was prepared using Millipore Milli-Q water. NaOH (GR for analysis) and Ethanol (LiChrosolv) were obtained from Merck.

2.3. Experimental details

Before the measurements, all solutions were deaerated by N_2 purging. All experiments were carried out at an overpressure of 3 bar and at temperatures between 23 °C and 90 °C (only for the Pt/C catalyst) or 100 °C (for the other catalysts), as indicated, using a Pine Instruments potentiostat (model AFRDE5). A flow rate of 15 μl s^{-1} was used as representative value [43].

The potentiodynamic measurements (10 mV s^{-1} scan rate) were performed by continuous cycling in the potential range between 0.06 and 1.16 V for the Pt/C and Pd/C electrodes, between 0.1 and 1.2 V for the $Pd/CeO_2/C$ electrode and between 0.06 and 0.8 V for the PtRu black electrode to avoid a possible electrochemical dissolution of Ru at higher potentials. The potentiostatic measurements were performed as follows: at the end of the cycling procedure, the potential was stopped at the low potential limit of 0.06 V during a negative-going scan, held there for 5 min, and then the potential was stepwise increased to higher potentials, first to 0.2 V, then in increments of 0.1 V. Each potential was held for a period of 300 s to approach steady-state conditions. Finally, the potential was stepped back to 0.06 V and held at this potential, until the Faradaic current reached a stable background level.

For the Pt/C catalyst, which appeared to be severely affected by the "history" of the previously applied potentials, we performed additional measurements using a slightly different experimental protocol, and the data presented in this paper will refer to this protocol. To avoid effects caused by differences in the initial state of the catalyst, it was first cleaned by stepping from 0.06 to 1.2 V to oxidatively remove adsorbed residues, followed by stepping back to 0.06 V. This inhibits the dissociative adsorption of ethanol by surface blocking by underpotentially deposited hydrogen. Finally the potential was stepped to the desired potential (between 0.4 and 0.7 V). This procedure was employed for each potential. Furthermore, the waiting time at each potential was extended to 15 min to obtain steady-state currents. To assess the initial oxidation rates, the double-layer charging current was determined in comparative experiments in ethanol-free 0.5 M supporting NaOH electrolyte under analogous experimental conditions on the Pt/C catalyst and then subtracted from the traces recorded in ethanol containing electrolyte.

The mass specific currents/active surface area specific current densities and the apparent activation energies for ethanol oxidation on different catalysts were calculated from the steady-state Faradaic currents during potentiostatic ethanol oxidation. For the Pt/C catalyst and selected potentials (0.4 and 0.5 V), we also derived these values from the double-layer charging corrected (see above) initial EOR currents.

3. Results and discussion

3.1. Pre-adsorbed CO_{ad} oxidation

The catalysts were characterized by electrochemical oxidation of a pre-adsorbed saturated CO adlayer (CO_{ad} stripping) and subsequent base voltammetry (1 cycle) in CO-free supporting 0.1 M NaOH electrolyte (Fig. 2(a)). The onset of CO_{ad} oxidation on the Pt/C catalyst is at ca. 0.2 V, which is ~0.2 V more negative compared with acidic solution on the same catalyst [19,21], and in agreement with previous data [44,45]. This can be related to more facile OH adsorption in alkaline medium. With further increase in the potential, the current passes through a pre-peak at ca. 0.3 V, a shoulder at ca. 0.5 V and the main peak with a maximum at ca. 0.62 V. The latter two features are attributed to CO_{ad} oxidation on Pt nanoparticle agglomerates and on separate nanoparticles [46–48]. A subsequent base voltammogram displays typical features of a Pt/C electrode in alkaline solution [20,49].

For saturated CO adlayer oxidation on an unsupported PtRu catalyst, the reaction starts at ca. 0.3 V, and passes through a single peak centered at ca. 0.52 V (Fig. 2(b)). Though PtRu is considered as a typical "bifunctional" catalyst in acidic media, it does not perform much better than pure Pt/C in alkaline electrolyte, due to the ability of the latter to adsorb OH and oxidize CO_{ad} even at relatively low potentials in alkaline solution. This reduces the advantages of the alloy catalyst over a monometallic one in acidic solution. CO_{ad} oxidation on a commercial Pd/C catalyst exhibits an ill-resolved onset at ca. 0.4 V, followed by a pre-peak at ca. 0.6 V and the main peak at ca. 0.83 V (Fig. 2(c)), in agreement with previous data [50]. Finally, the Pd-based catalyst supported over a mixed oxide/carbon support shows a pronounced main peak at ca. 0.82 V. An ill-resolved pre-peak may appear at lower potential, where it would interfere with absorbed hydrogen oxidation (Fig. 2(d)). Interestingly, for the latter catalyst a pronounced reduction peak appears at ca. 0.62 V in the first negative-going scan after CO_{ad} oxidation, which can be attributed either to PdO reduction [51] or the reduction of non-stoichiometric CeO_x formed at higher potentials.

The CO_{ad} oxidation charge, estimated from the integration of the current difference between the first positive-going and the subsequent second scan results in the following electrochemically active surface areas for the different catalysts: 1.5, 0.15, 0.78 and 0.6 $cm^2\ \mu g_{Me}^{-1}$ for the Pt/C catalyst, the PtRu black catalyst, the Pd/C catalyst and the $Pd/CeO_2/C$ catalyst, respectively. These values were used for calculating the intrinsic active surface area normalized activities for ethanol oxidation at constant potentials (Section 3.4).

The base CVs of the respective catalysts agree well with those reported in previous studies on similar type electrodes.

3.2. Potentiodynamic oxidation of ethanol

Fig. 3 shows a series of potentiodynamic ethanol oxidation traces recorded during continuous potential cycling (10 mV s^{-1} scan rate) in 0.5 M NaOH solution containing 0.1 M ethanol on different catalysts and at different temperatures (see figure): (a) Pt/C catalyst, (b) PtRu black, (c) Pd/C and (d) $Pd/CeO_2/C$ catalysts, respectively. For more clarity, the positive-going scans and the negative-going scans are displayed in two separate panels. (It should be noted that the absence of curves for Pt/C and for Pd/C catalysts in the negative-going scan at 100 °C is due to the appearance of instabilities/oscillations.) In addition, the traces recorded at room temperature are also shown with higher magnification for better comparison (magnifications see figures). Furthermore, the onset of the Faradaic currents in the positive-going scan is shown in the insets in an expanded current scale.

For the Pt/C catalyst (Fig. 3(a)) at 23 °C, the general pattern of the Faradaic current is similar to that reported previously for

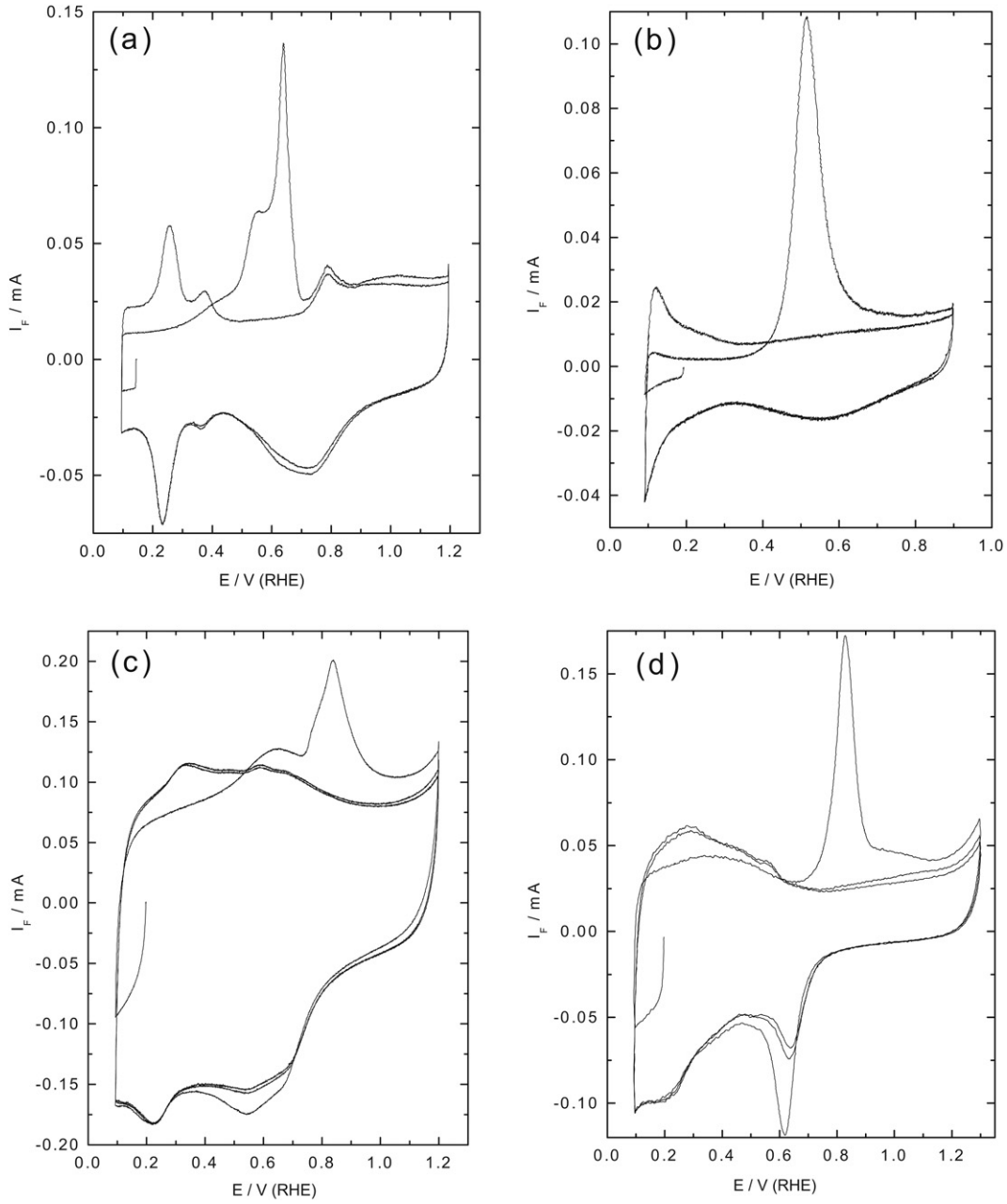

Fig. 2. Voltammetric profiles for CO adlayer stripping and the subsequent base voltammograms on (a) Pt/C, (b) PtRu black, (c) Pd/C and (d) Pd/CeO_2/C catalysts in 0.1 M NaOH solution at room temperature. Potential scan rate 10 mV s^{-1}.

a similar Pt/C catalyst and under similar reaction conditions [20]. At potentials below about 0.28 V (see inset), the electrooxidation of ethanol is essentially inhibited, due to the presence of a reaction inhibiting adlayer of adsorbed residues resulting from dissociative ethanol adsorption, which was formed at lower potentials in the preceding negative-going scan. These adsorbates are mainly CO_{ad} and adsorbed hydrocarbon residues [19,21]. However, compared to results reported previously in acidic electrolyte (at identical transport and reaction conditions, 0.5 M H_2SO_4 solution [52]), the onset potential is shifted to lower values (0.28 V in alkaline electrolyte vs. 0.35 V in acidic electrolyte at 23 °C), which is attributed to the more facile OH^- adsorption from alkaline electrolyte as compared to OH_{ad} formation from H_2O electrosorption in acidic electrolyte [27,53,54].

At potentials above 0.28 V, the Faradaic current increases, which correlates with the onset of CO_{ad} oxidation on Pt electrodes in alkaline electrolyte (Fig. 2(a) [44]), passes through a maximum at ~0.56 V, and then decreases with further increasing potential through an ill-resolved shoulder between 0.65 and 0.75 V (see magnified current trace). This agrees well with previous reports on CO_{ad} oxidation on a Pt electrode in alkaline solution [44,55–58]. With further increasing potential, the Faradaic current decays continuously, until reaching very small values at a potential above 0.9 V. This decay is related to the increasing coverage of OH_{ad}/surface oxide species, which inhibit the adsorption/oxidation of ethanol.

Increasing the temperature from 23 to 90 °C, we observed the following characteristic changes in the positive-going scan: *i)* the

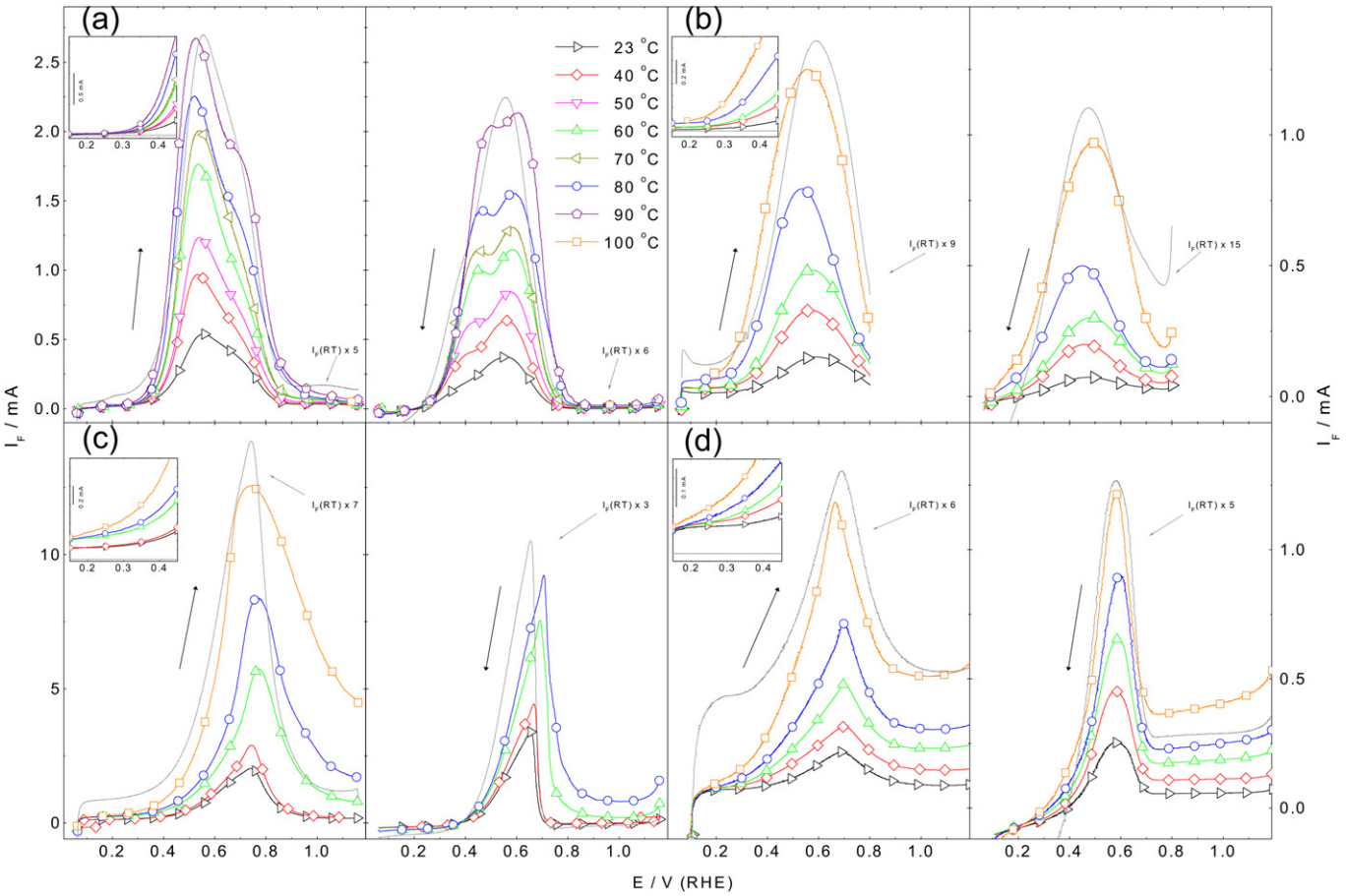

Fig. 3. Positive-going scan (left panel) and negative-going scan (right panel) of CVs of the ethanol oxidation reaction during continuous potential cycling on different thin-film catalyst electrodes in 0.1 M ethanol + 0.5 M NaOH solution pressurized with 3 bar N_2 overpressure at elevated temperatures (temperatures see figure): (a) Pt/C catalyst, (b) PtRu black catalyst, (c) Pd/C catalyst and (d) Pd/CeO_2/C catalyst. Inset: onset of the reaction magnified Faradaic current. Potential scan rate 10 mV s^{-1}, electrolyte flow rate 15 μl s^{-1}, arrows indicate the direction of potential scan.

peak current increases by a factor of five, *ii)* the onset potential shifts negatively, from ~0.28 to ~0.24 V, *iii)* the potential of the peak maximum shifts from ~0.56 to ~0.52 V, and *iv)* the ratio between the peak current and the current in the ill-resolved shoulder increases slightly with temperature. The obvious thermal activation of the EOR, which agrees with similar tendencies in the temperature dependent EOR in acidic electrolyte [52], can result from different effects, including the activation of the C–C dissociation, partial thermal desorption of CO_{ad} species formed during the reaction [59], and/or activation of the reaction between ethanol adsorbates and oxygen-containing species [60–62].

The general appearance of the current trace in the negative-going scans (Fig. 3(a), right panel), resembles that in the positive-going scans (Fig. 1(a), left panel). At potentials above ~0.8 V (at 23 °C), the reaction is inhibited by surface oxide species, while upon their reduction the Faradaic current increases until reaching its maximum at ca. 0.56 V, then decreases through an ill-resolved shoulder at ca. 0.37 V, and finally reaches very small values. With increasing temperature, the Faradaic current peak develops a distinct double-peak characteristics (the shoulder becomes more pronounced) and the peak current increases by about a factor of four at 90 °C compared to that at ambient temperature. Furthermore, the ratio of the peak currents in the negative-going scan and in the positive-going scan ($I_{F,n}/I_{F,p}$) increases from 0.7 at 23 °C to 0.8 at 90 °C, most likely due to differences in the respective coverages of adsorbed ethanol decomposition products formed at lower potentials in the preceding negative-going scans. Similar observations ($I_{F,n}/I_{F,p} < 1$) were reported for the oxidation of methanol on a polycrystalline Pt electrode in alkaline solution, where the $I_{F,n}/I_{F,p}$ ratio was used as an estimate of the poisoning effect, which caused a decrease of the current in the negative-going scan. The decrease was ascribed to (bi)carbonate formation/adsorption [63]. One should consider, however, that the interpretation of the peak intensity ratio, which was used as a simplified criterion for surface poisoning, is not straightforward, since it can largely depend on experimental parameters such as the potential scan rate, which affects the adsorbate formation and oxidation, or the resistance of the solution, which can modify the peak currents via Ohmic drop effects. Thus we consider this parameter more as a qualitative indicator.

For the PtRu black catalyst electrode (Fig. 3(b)), the general appearance of the Faradaic current profiles is rather similar to that of the Pt/C catalyst. The main temperature-induced effects (23 °C vs. 100 °C) can be summarized as follows: *i)* the peak current in the positive-going scan increases by a factor of 7, *ii)* the onset potential shifts negatively (~0.25 V vs. ~0.20 V). Here it should be noted that compared with the onset value of 0.3 V on a PtRu/C catalyst electrode in 0.5 M H_2SO_4 solution (0.1 M ethanol, room temperature) [64], the change in pH from 0.3 to 13.7 results in a negative potential shift of ~50 mV. *iii)* Different from the Pt/C catalyst, the Faradaic current for ethanol oxidation on the PtRu black catalyst shows a single broad peak, and the peak potential shifts only by ca.

30 mV, from ~0.58 V at 23 °C to ~0.55 V at 100 °C. The current–potential profiles closely resemble also those reported for methanol oxidation on a PtRu alloy catalyst at different temperatures in alkaline solution [65]. Similar thermally induced shifts of the onset potential were observed in earlier temperature dependent studies of methanol oxidation on PtRu alloy electrodes in acid [66] and in alkaline electrolyte [27]. The lower onset potential compared to a Pt/C catalyst is commonly attributed to an easier formation of oxygen-containing species on the Ru sites at low potentials, although these effects are much smaller than in acidic electrolyte (see Section 3.1), together with modifications of the Pt electronic states by alloyed Ru, resulting in a weaker adsorbate bonding to Pt [67,68]. On the other hand, the lower Faradaic current compared to that on the Pt/C catalyst, illustrated, e.g., by a peak current of 0.8 mA on PtRu black vs. 2.3 mA on the Pt/C catalyst (both at 80 °C), points to a kinetic hindrance of the EOR on the PtRu catalyst. This is most easily explained by a slower ethanol adsorption/dehydrogenation reaction on the Ru sites or, more likely, on Pt sites modified by electronic ligand and strain effects. A similar observation of an earlier onset of the reaction on PtRu was reported for methanol electrooxidation on a PtRu/C catalyst in both alkaline and acidic solution [27].

Considering that CO_{ad} oxidation starts at almost identical potentials on Pt/C and PtRu in alkaline solution (see Section 3.1, Fig. 2(a) and (b)), the earlier onset of the EOR on the PtRu catalyst can not be explained by a more facile removal of electrode poisoning CO_{ad} only. It rather points to a more hindered CO_{ad} formation over the bimetallic catalyst. In that case, the earlier onset of the EOR over the PtRu catalyst can result from an increased incomplete ethanol oxidation on the accessible surface. The latter was concluded also for the reaction on the PtRu/C catalyst in acidic medium [69].

The negative-going Faradaic current scans resemble the positive-going scans in their general appearance (Fig. 3(b)); the $I_{F,n}/I_{F,p}$ ratios remain well below 1 (0.53 at 23 °C, 0.78 at 100 °C). Most likely, this reflects a considerable influence of the high CO_{ad} coverage present in the initial stage of the positive-going scan, while in the initial phase of the negative-going scan the CO_{ad} coverage is negligible. In addition, the different composition/coverage of the adlayer may affect also the selectivity of the reaction [52], with direct consequences for the measured Faradaic current.

For the Pd/C catalyst (Fig. 3(c)), at 23 °C and in the positive-going scan, the Faradaic current starts at ca. 0.32 V, passes through a maximum at about 0.74 V, and then decreases with further increasing potential, until reaching its minimum value at about 1.0 V, similarly to findings in Ref. [37]. The later onset of the EOR on the Pd/C catalyst compared to the Pt/C catalyst agrees with the later onset of CO_{ad} oxidation on the Pd/C catalyst (Fig. 2(c)). The decrease in Faradaic current at potentials > 0.74 V is related to the formation of a OH adlayer or Pd oxide layer on the electrode surface [36,70–72]. With increasing temperature, the Faradaic current increases and the onset potential shifts to lower values, reaching 0.27 V at 100 °C. In the subsequent negative-going scan, the general current–potential profile is characterized by a sharp peak at ca. 0.66 V (at 23 °C), whose peak potential shifts to higher potential with increasing temperature, reaching about 0.7 V at 80 °C. The corresponding $I_{F,n}/I_{F,p}$ ratio decreases from 1.7 at 23 °C to 1.1 at 80 °C.

Finally, for the $Pd/CeO_2/C$ catalyst (Fig. 3(d)), the onset potential is shifted negatively compared to the Pd/C catalyst, from ~0.32 V (Pd/C) at 23 °C to ~0.2 V. Obviously, the presence of CeO_2 promotes the oxidation of ethanol at lower potentials, which can be explained by the ability of ceria and ceria related materials to store and release oxygen [73]. It can provide O-containing species, which facilitate the oxidation of reaction inhibiting adspecies. Notably, there is no significant shift of the onset potential for CO_{ad} oxidation on $Pd/CeO_2/C$ and Pd/C catalysts (Fig. 2(c) and (d), respectively). Therefore, the dissociative adsorption of ethanol over $Pd/CeO_2/C$ catalyst can be hindered, allowing for the onset of incomplete ethanol oxidation. With increasing reaction temperature, *i)* the onset potential shifts to slightly lower values, reaching ~0.15 V at 100 °C, *ii)* the peak potential shifts from ~0.7 V at 23 °C to 0.66 V at 100 °C, and *iii)* the peak current for ethanol oxidation increases by a factor of 5.4 from 23 °C to 100 °C. After passing through the maximum, the current decays slowly and reaches a plateau at ~1.0 V at 23 °C (at ~0.9 V at 100 °C). Hence, similar to the Pd/C catalyst, $Pd/CeO_2/C$ catalyzes the EOR at high potentials, where the metal surface is covered by OH_{ad} or surface oxide. This tendency is most pronounced for the present catalyst. In the negative-going scan, the general appearance of the current trace is rather similar to that in the positive-going scans.

The peak currents are almost identical in the two scan directions, with the ratio $I_{F,n}/I_{F,p}$ decreasing from 1.14 at 23 °C to 1.03 at 100 °C, reflecting a more effective thermal activation of the reaction in the positive-going scan (an increase by factor of 5.5 in the positive-going scan vs. 4.9 in the negative-going scan, both comparing I_F at 100 °C with that at 23 °C). Following the arguments given above for Pt/C, the $I_{F,n}/I_{F,p} \approx 1$ indicates that the influence of the adlayer, including coverage and composition, on the overall Faradaic current is little.

Overall, the potentiodynamic data showed a pronounced effect of the temperature not only on the absolute currents, but also on details of the shape of the CVs, indicating the coexistence and competition of several activated reaction steps.

3.3. Potentiostatic oxidation of ethanol

In order to separate kinetic (reaction rate) and dynamic (temporal variation of the electrode potential) contributions to the Faradaic current in the potentiodynamic measurements, e.g., via time and potential dependent adsorbed species coverages, we performed a series of potentiostatic experiments (for details see Section 2.3) at different electrode potentials/reaction temperatures in 0.5 M NaOH solution containing 0.1 M ethanol (Fig. 4). Generally, the Faradaic current was followed over 300 s at each potential, and the potential was increased stepwise. Only for the Pt/C catalyst, this was extended to 900 s to reach steady-state conditions, and all transients started from 0.06 V (details see Section 2.3). Arrhenius plots of the steady-state Faradaic currents for determining the apparent activation energies are presented and discussed in Section 3.5.

For the Pt/C catalyst (Fig. 4(a)), the ethanol oxidation transients show a steep initial increase after the potential step, followed by a slower, approximately exponential decrease to approach the steady-state current. The initial spike, which is partly due to double-layer charging, as well as the currents in the later stages of the transients, depend sensitively on temperature and reaction potential. The profiles of the initial current maximum become progressively sharper with increasing temperature, with the rapid increase of the Faradaic current at higher temperature followed by an almost equally fast decay, due to the rapid development of reaction inhibiting adsorbed species such as adsorbed CO or other strongly bonded species originating from the dissociative adsorption of ethanol under these conditions [19,21], while at 23 °C the Faradaic current increases slowly followed by a slow decay.

At 0.4 and 0.5 V (Fig. 4(a)), the reaction exhibits an unusual temperature dependence: at lower temperatures, from 23 to 80 °C, the steady-state Faradaic current decreases with increasing temperature, and only when going 90 °C it increases again. This is possibly due a change in the origin of the rate limitation, from site blocking due to increasing CO_{ad} formation and coverage at lower temperatures to CO_{ad} formation at 90 °C.

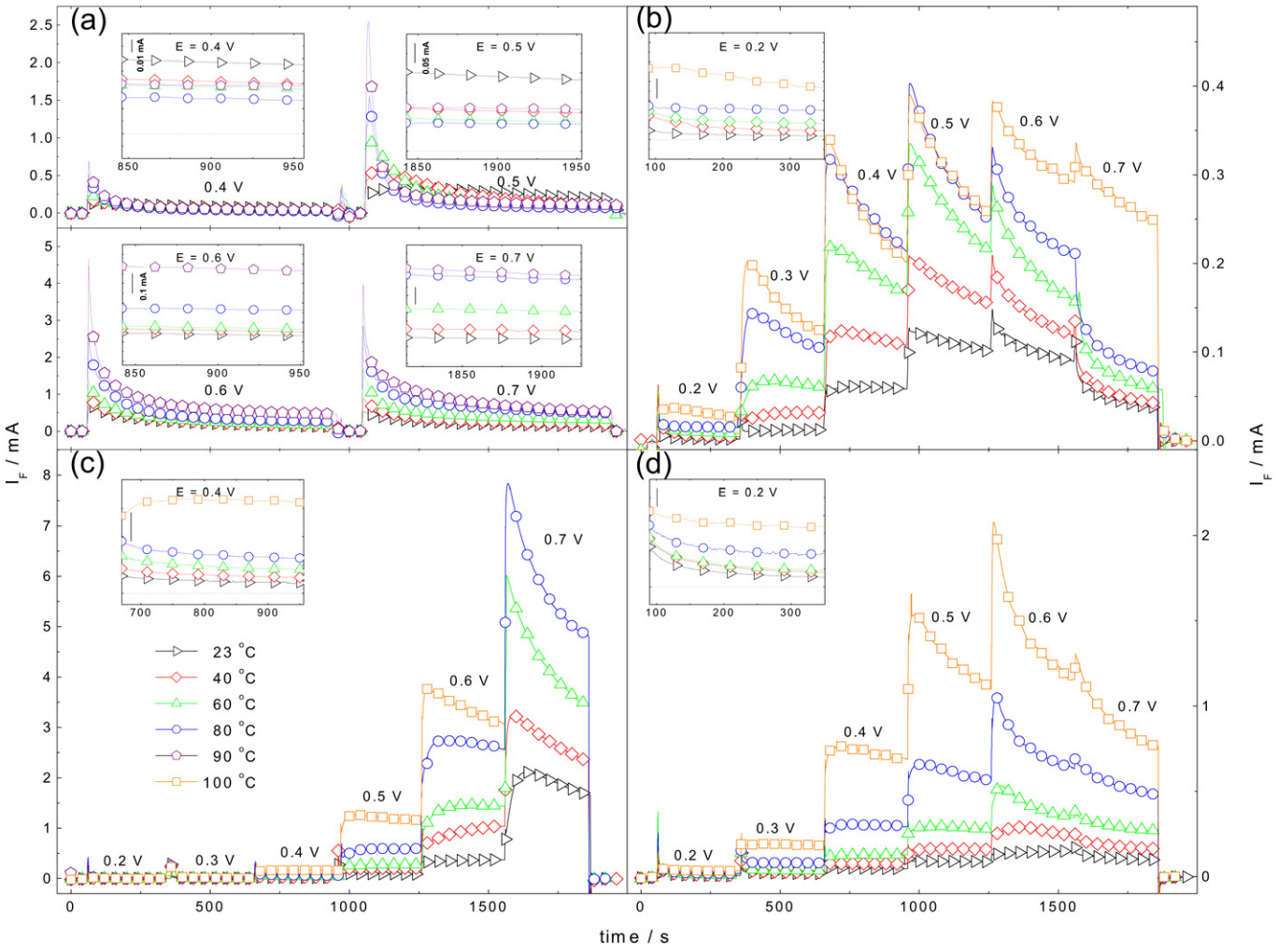

Fig. 4. Recorded transients of the Faradaic current during potentiostatic oxidation of ethanol on different catalyst electrodes: (a) Pt/C catalyst, (b) PtRu black catalyst, (c) Pd/C catalyst and (d) Pd/CeO_2/C catalyst in 0.1 M ethanol + 0.5 M NaOH solutions. Temperatures see figure, electrolyte flow rate 15 μl s^{-1}.

Comparable potentiostatic measurements of the ethanol oxidation reaction on a Pt/C catalyst at 0.4, 0.5 and 0.6 V (15 min for each step) over the temperature range from 22 to 60 °C were reported recently [20]. For reaction at 0.4 V and 0.5 V, those authors observed that the oxidation current density increased when raising the temperature from 22 to 40 °C, and then decreased upon a further temperature increase to 60 °C. They explained this by the temperature dependent coverage of poisoning species on the catalyst surface, which increases with increasing temperature, resulting in lower currents at 60 °C than at 23 °C. Studying the adsorption, dehydrogenation and oxidation of methanol on Pt(111) in alkaline solution, Spendelow et al. identified CO_{ad} as the main poisoning species, which affects the methanol dehydrogenation rate as well as the CO_{ad} oxidation rate as the main limiting step [74]. A study of the role of OH_{ad} species and of the influence of anions in the methanol oxidation on a Pt electrode in different alkaline solutions (NaOH, Na_2CO_3 and $NaHCO_3$) revealed that adsorption of carbonate and bicarbonate on the electrode surface reduce the extent of OH adsorption and the activity of the electrode [75]. Comparable findings on the effect of carbonate/bicarbonate adsorption were reported by Tripkovic et al. [76].

At 0.6 and 0.7 V reaction potential, the temperature dependence of the steady-state ethanol oxidation currents on the Pt/C catalyst reverts to a 'normal' Arrhenius behavior. In both cases, the current increases by a factor of ~4 when increasing the temperature from 23 to 90 °C. The change in reaction behavior compared to the lower reaction potentials is related to differences in the nature and stability of the adlayer of adsorbed reaction intermediates/side products formed during reaction. The formation of such species is known to be potential dependent [21], with the incomplete oxidation product acetate prevailing at higher potential [17,22].

The current transient profiles measured on the PtRu black catalyst (Fig. 4(b)) generally resemble those measured on the Pt/C catalyst, with the exception that the reaction times at each potential were shorter (300 s) and that the different potentials were measured sequentially, stepping the potential to increasingly higher potential. The main characteristics can be summarized as follows: *i)* the onset potential is at about 0.2 V, i.e., ~100 mV downshifted compared with Pt/C. *ii)* The Faradaic current increases with increasing temperature at all potentials, different from the inverse behavior of the Pt/C catalyst at low potentials (0.4 and 0.5 V). *iii)* The increase depends significantly on the reaction potential. Furthermore, at 0.4 V and 0.5 V, the Faradaic current increases more steeply in the lower temperature range, from 23 to 60 °C, than at higher temperatures, from 80 to 100 °C (see also Section 3.4), The latter behavior can be tentatively explained by a faster oxidation of CO_{ad} or $CH_{x,ad}$ species to (bi)carbonate in the lower temperature regime, due to increasing OH_{ad} formation on

the Ru sites and thus while at 80 and 100 °C, excessive formation of OH_{ad} increasingly hinders the dissociative adsorption/oxidation of ethanol and thus limits the current. *iv)* Going from 0.6 to 0.7 V, the Faradaic current decreases at all temperatures, again due to the increased oxide formation on the PtRu surface. *v)* The absolute values of the Faradaic currents on the PtRu black film electrodes are significantly lower than those obtained on the Pt/C film electrodes. This will be discussed in more detail in Section 3.4, when considering the intrinsic activities (active surface area normalized current densities).

For the Pd/C catalyst (Fig. 4(c)), we found a measurable Faradaic current for all temperatures at 0.4 V (see inset in Fig. 4(c)). At potentials of 0.4 V and 0.5 V, the Faradaic current–time profiles reach a stable value within 8 s after the potential step at all temperatures, which is very different from the rapid initial decay observed for the Pt/C and PtRu catalysts. (Fig. 4(a) and (b)). Obviously, the Pd/C catalyst is less susceptible to poisoning by adsorbed reaction intermediates/side products, which agrees well with reports that acetate is the major reaction product on this catalyst [30,39,40,77,78]. For instance, less than 5% of the ethanol is converted to the complete oxidation product (carbonate) in 1.0 M KOH solution containing 1 M ethanol on a Pd/C catalyst at room temperature [36]. At 0.6 V, the current profiles resemble those at 0.5 V below 60 °C, except for the higher absolute current values, while at higher temperatures (80 and 100 °C), they exhibit an increasing deactivation tendency. The measurements at 100 °C for 0.7 V are not included due to the extensive gas evolution at the counter electrode, which causes instabilities in the measured current and finally loss of the contact to the counter electrode.

For the $Pd/CeO_2/C$ catalyst (Fig. 4(d)), we find a measurable Faradaic current increase with increasing temperature already at a potential of 0.2 V (see inset in Fig. 4(d)), similar to the PtRu black catalyst. The rapid build-up of stable current–time profiles at 0.3 and 0.4 V after the potential step indicates a high stability toward poisoning by strongly adsorbed species, either due to a low C–C bond breaking rate, i.e., prevailing incomplete oxidation, or due to more facile removal of these adsorbates. At 0.5 V, the ethanol oxidation rate reaches a stable value simultaneously with the potential step at lower temperature (below 80 °C) and decays slowly at higher temperatures. At 0.6 V, these characteristics are even more pronounced than at 0.5 V, with an even steeper increase and a faster decay in Faradaic current. Stepping the potential from 0.6 to 0.7 V at the respective temperature has little effect on the Faradaic current, it continues to decrease with time, continuing the decay observed at 0.6 V. The different characteristics of the Faradaic current changes upon stepping the potential from 0.6 to 0.7 V compared to that of the Pd/C catalyst are possibly due to the higher abundance of oxygen-containing species on $Pd/CeO_2/C$ catalyst.

Comparison between the Pt/C and PtRu black catalysts on the one hand and between the Pd/C and $Pd/CeO_2/C$ catalysts on the other hand shows that the addition of the oxophilic components Ru to Pt and CeO_2 to the Pd/C catalyst increases the tolerance toward poisoning at lower potentials in the potentiostatic and potentiodynamic measurements. This can be explained by the ability of CeO_2 and Ru to supply oxygen-containing species at low potentials, which improves the oxidation of catalyst poisoning CO_{ad} species. Similar as in acidic medium, acetaldehyde (in the form of diolate in alkaline medium), acetic acid (acetate ion in alkaline medium) and carbon dioxide ((bi)carbonate in alkaline environment) are considered as reaction products in the EOR in alkaline electrolyte, which are also detected by electrochemical methods combined with other techniques, such as HPLC [22] or *in situ* Fourier transform infrared spectroscopy (FTIR) [37,79]. The severe poisoning of the Pt/C catalyst is ascribed to strongly adsorbed species such as CO_{ad} or $CH_{x,ad}$ species. On the other hand, the higher activity of the Pd/C catalyst may be due to its lower poisoning, due to a lower ability for C–C bond dissociation, which results in a higher tendency for incomplete oxidation of ethanol, mainly to acetate in alkaline solution [35,79–81]. This can also explain the different ratios of the peak currents in the positive- and negative-going scan mentioned above (see Section 3.2): For the Pt/C catalyst, the stable adsorbed species, mainly CO_{ad}, will block active surface sites in the positive-going scan, but much less in the negative-going scan, while for the Pd/C catalyst, CO_{ad} formation/oxidation is less pronounced [35,79].

Comparing the potential and temperature dependence of the Faradaic current for the different catalysts, we find the highest current for the Pt/C catalyst at 0.5 V at 23 °C, while at 80 °C a further potential increase still leads to increasing currents (maximum current at 0.7 V). For the Pd/C catalyst, the best performance was obtained at 0.7 V for both temperatures. For the PtRu black catalyst, the Faradaic current reaches its maximum value at 0.5 V and decreases at higher potentials of 0.6 and 0.7 V, also for both temperatures. Finally, the $Pd/CeO_2/C$ catalyst reaches its maximum current at 0.6 V.

In total, the temperature and potential dependent behavior indicates an increasing activation of the EOR on both Pt-based and Pd-based catalysts with temperature, the differences in the ethanol oxidation reaction characteristics on Pt-based catalyst vs. Pd-based are mainly attributed to differences in the activity for C–C bond breaking and the resulting formation/removal of reaction inhibiting adsorbates. Generally, the steady-state currents achieved at constant potentials between 0.3 and 0.6 V are significantly lower than those appearing in potentiodynamic experiments at the corresponding potentials (see Fig. 3). This is due to the different coverages of the various adsorbed species, where steady-state coverages are reached only after longer times. Only at very low potentials, where the reaction is essentially inhibited by a high coverage adlayer, or at high potentials, where oxy-adspecies dominate the surface, there is little difference between potentiodynamic and potentiostatic currents. This underlines the importance of the composition and the coverage of the adlayer developed in both situations for the measured reaction activity and, presumably, also the selectivity. Therefore, for the kinetic evaluation the better defined values derived under steady-state conditions at constant potentials will be used in the following. In addition, these conditions are also more relevant for comparison with fuel cell operation.

3.4. Mass specific currents and active surface area specific current densities

In order to exclude any influence of the different metal loadings and the electrochemical active surface areas of the respective catalysts on the ethanol oxidation activity, the steady-state Faradaic currents in Fig. 4 were converted into metal mass specific currents (Fig. 5(a) and (b)) and active surface area specific current densities (Fig. 5(c) and (d)). The values resulting for 23 °C (upper panels) and 80 °C (lower panels) are presented in Fig. 5, a complete compilation of the values is given in Table 1. The activities at low potentials (0.2 and 0.3 V) are also shown in larger magnification for better identification. In addition, the active surface area normalized currents are a measure of the intrinsic activities of the respective catalysts, which are not accessible from the commonly used mass specific activities.

For the technically relevant metal mass specific activities, measurable currents were detected at the lowest potential of 0.2 V on the PtRu black and $Pd/CeO_2/C$ catalysts, both at 23 °C and 80 °C (see insets in Fig. 5(a) and (b)), with the latter showing a higher mass specific activity. At 0.3 V, both mass specific activities increase compared to those at 0.2 V.

At 0.4 V, the mass specific activity decreases in the order $Pt/C > Pd/CeO_2/C >$ PtRu black $> Pd/C$ at 23 °C, while at 80 °C this

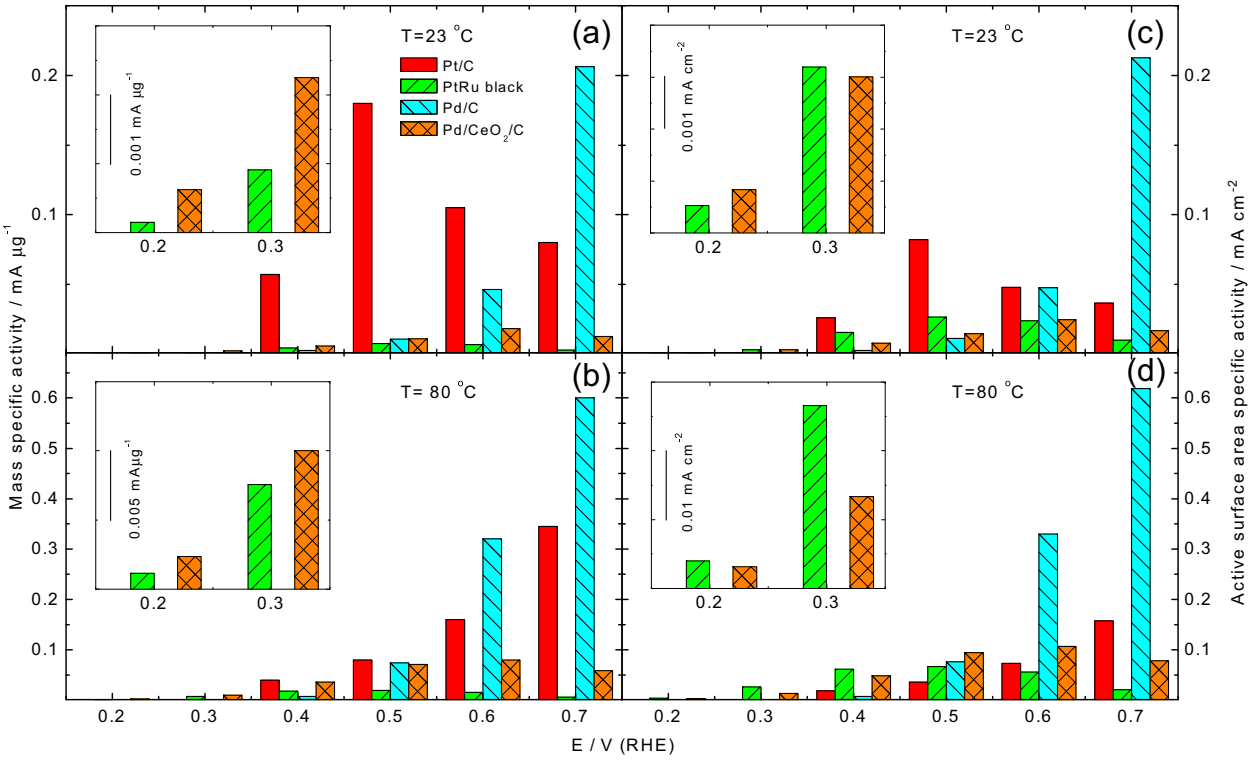

Fig. 5. Mass specific (a, b) and active surface area specific (c, d) activities during potentiostatic oxidation of ethanol on the different catalysts: Pt/C, PtRu black, Pd/C and $Pd/CeO_2/C$ (for assignments see figure) in 0.1 M ethanol + 0.5 M NaOH solutions at 23 °C (upper panel) and 80 °C (lower panel). Electrolyte flow rate 15 μl s^{-1}.

order has changed to $Pd/CeO_2/C > PtRu\ black > Pt/C > Pd/C$. The unusual temperature dependence of the Pt/C catalyst, with a current decrease with increasing temperature, is of course observed also in the mass specific currents, while for the other catalysts the mass specific current increases with temperature, by a factor of 4 for the PtRu black catalyst, 3 for the Pd/C catalyst and 6 for the $Pd/CeO_2/C$ catalyst. At 23 °C, the mass specific current density is highest on the Pt/C catalyst up to 0.6 V, and only at 0.7 V the Pd/C catalysts performs better, by almost a factor of 3. In contrast, at 80 °C, the Pd/C catalyst shows the highest mass specific activity already at 0.5 V, and at 0.7 V it is more than a factor of 2 better than that of the Pt/C catalyst. Hence, at technically relevant conditions (continuous electrolyte flow, constant potential, elevated temperature), the Pd/C catalyst shows the highest activity at potentials ≥ 0.5 V. Only at lower potentials (0.2–0.4 V), other catalysts perform better under these conditions. At 0.5 V, the difference between Pd/C and $Pd/CeO_2/C$ catalysts is small. These results clearly point to an improved performance of the Pd/C catalyst compared to the Pt/C catalyst under technically relevant conditions. Addition of CeO_2 as oxophilic co-catalyst results in further improvement only at low potentials (≤0.4 V).

The intrinsic active surface area normalized activities (active surface area normalized current densities, Fig. 5(c) and (d)) show slightly different characteristics as compared to the mass specific activities, due to the differences in active surface area of the different catalysts. Compared to the trends in metal mass specific currents, the main differences are *i)* the even more distinct difference in activity between Pd/C and Pt/C catalysts, with the former one showing a better performance at ≥0.6 V at 23 °C and at ≥0.4 V at 80 °C and *ii)* the somewhat higher activity of the 'bimetallic' PtRu black and $Pd/CeO_2/C$ catalyst. At low potentials, at ≤0.4 V at 23 and at 80 °C, respectively, they show the highest activity, underlining the role of the oxophilic second component at low potentials.

Table 1
Metal mass specific currents *i* and active surface area specific current densities *j* in the EOR on the different catalysts at different potentials, determined from steady-state reaction currents in Fig. 4.

Catalyst	Reaction potential/V_{RHE}											
	0.2			0.3		0.4		0.5		0.6		0.7	
	T/ °C	*i*/mA μg_{Me}^{-1}	*j*/mA cm^{-2}	*i*/mA μg_{Me}^{-1}	*j*/mA cm^{-2}	*i*/mA μg_{Me}^{-1}	*j*/mA cm^{-2}	*i*/mA μg_{Me}^{-1}	*j*/mA cm^{-2}	*i*/mA μg_{Me}^{-1}	*j*/mA cm^{-2}	*i*/mA μg_{Me}^{-1}	*j*/mA cm^{-2}
Pt/C	23	–	–	–	–	0.027	0.03	0.1	0.08	0.07	0.05	0.08	0.04
	80	–	–	–	–	0.014	0.02	0.04	0.04	0.13	0.07	0.25	0.16
PtRu black	23	0.0002	0.0005	0.001	0.003	0.004	0.02	0.008	0.03	0.007	0.024	0.003	0.01
	80	0.0011	0.004	0.008	0.027	0.017	0.06	0.019	0.07	0.016	0.056	0.006	0.02
Pd/C	23	–	–	–	–	0.002	0.003	0.01	0.01	0.05	0.05	0.2	0.21
	80	–	–	–	–	0.007	0.008	0.074	0.08	0.32	0.33	0.6	0.62
$Pd/CeO_2/C$	23	0.0006	0.0008	0.002	0.003	0.006	0.008	0.011	0.015	0.02	0.025	0.013	0.02
	80	0.0024	0.003	0.01	0.013	0.036	0.048	0.071	0.095	0.08	0.11	0.06	0.08

3.5. Apparent activation energies

The apparent activation energies E_a for the ethanol oxidation reaction, determined from temperature dependent steady-state Faradaic currents at the respective reaction potentials, were calculated from the Arrhenius plots in Fig. 6. The resulting values are listed in Table 2. For the Pt/C catalyst, which showed a decrease of the steady-state Faradaic current with temperature at 0.4 and 0.5 V, we used the initial maximum currents at these potentials, after correction for double-layer charging, to obtain activation energies reflecting the inherent activities rather than the blocking by stable adsorbates (see below).

The plots of the logarithmic oxidation rates vs. $1/T$ in Fig. 6 generally show a linear dependence, perhaps with the exception of the Pt/C catalyst, where the highest temperature values (90 °C) seem to deviate at all potentials. This implies that, in most cases the rate determining step does not change over the entire temperatures range.

The apparent activation energies of the EOR on the Pt/C catalyst electrode are 15 ± 4 kJ mol^{-1} and 20 ± 1 kJ mol^{-1} at 0.6 V and 0.7 V, respectively (see Table 2). As mentioned in Section 3.3, at 0.4 and 0.5 V the steady-state Faradaic currents decrease on this catalyst with increasing temperature up to 80 °C, which is equivalent to a negative activation energy. This was tentatively attributed to an increasing blocking of the surface by stable adsorbates, rather than to a negative barrier in an elemental reaction step (see Section 3.3). In order to assess the inherent activity of the material, we evaluated the temperature dependent initial currents (initial current maxima), after correction for double-layer charging (see Fig. 6(a)). The resulting currents yield values for E_a of 26 ± 4 kJ mol^{-1} at 0.4 V and 32 ± 4 kJ mol^{-1} at 0.5 V, respectively, which fit well to the data obtained at higher potentials (see Table 2). Because of the different schemes for evaluation, however, quantitative considerations of the potential dependence are hardly possible for this catalyst. For the PtRu black catalyst, the values for E_a first decay continuously with potential, from 30 ± 1 kJ mol^{-1} at 0.2 V to the minimum value of 11 ± 2 kJ mol^{-1} at 0.5 V. With further increasing potential, E_a increases again to 20 ± 6 kJ mol^{-1} at 0.7 V (see Table 2).

Table 2
Apparent activation energies for ethanol oxidation at different potentials, determined from steady-state reaction currents (see Fig. 4).

Catalyst	Potential					
	0.2 V	0.3 V	0.4 V	0.5 V	0.6 V	0.7 V
Pt/C	–	–	26 ± 4*	32 ± 4*	15 ± 4	20 ± 1
PtRu black	30 ± 1	28 ± 3	15 ± 3	11 ± 2	14 ± 1	20 ± 6
Pd/C	–	–	24 ± 3	29 ± 3	24 ± 3	17 ± 1
Pd/CeO_2/C	21 ± 3	28 ± 4	32 ± 3	30 ± 1	24 ± 2	24 ± 1

It should be noted that the apparent activation energies derived from the Faradaic currents in the potentiodynamic measurements differ considerably from those determined from the potentiostatic measurements, which is mainly due to the very different adlayer conditions.

These data can be compared with results obtained for related systems under comparable reaction conditions. Jiang et al. reported apparent activation energies for the EOR on a Pt/C catalyst in the range of 25–42 kJ mol^{-1} in 0.1 M NaOH solution containing 0.01 M ethanol (temperature range: 22, 40 and 60 °C, potential range 0.4–0.6 V_{RHE}) based on both potentiodynamic and potentiostatic measurements [20]. Investigating the EOR kinetics on Pt/C and PtPdAu/C catalysts in the temperature range of 20–80 °C in 0.5 M NaOH containing 1.0 M ethanol by potentiostatic measurements, Datta et al. obtained apparent activation energies on the Pt/C catalyst in the range of 9.0–13.6 kJ mol^{-1} at reaction potentials between 0.52 and 1.12 V_{RHE} (−0.4 and 0.2 V vs. Hg–HgO) [80]. It should be noted that the values of the apparent activation energies for ethanol oxidation on the Pt/C catalyst are significantly lower in alkaline electrolyte than in acidic environment [52]. Under otherwise similar reaction condition, we obtained E_a values of 41 ± 2 kJ mol^{-1} and 40 ± 2 kJ mol^{-1} at potentials of 0.58 and 0.68 V, respectively, in 0.1 M ethanol solution containing 0.5 M H_2SO_4, compared to 15 ± 4 kJ mol^{-1} and 20 ± 1 kJ mol^{-1} at 0.6 V and 0.7 V in alkaline electrolyte. At 0.6 V, oxidative removal of CO_{ad} is facile on the Pt/C catalyst due to sufficient formation of adsorbed hydroxyl species, and at 0.7 V, CO_{ad} oxidation is very fast. Under these

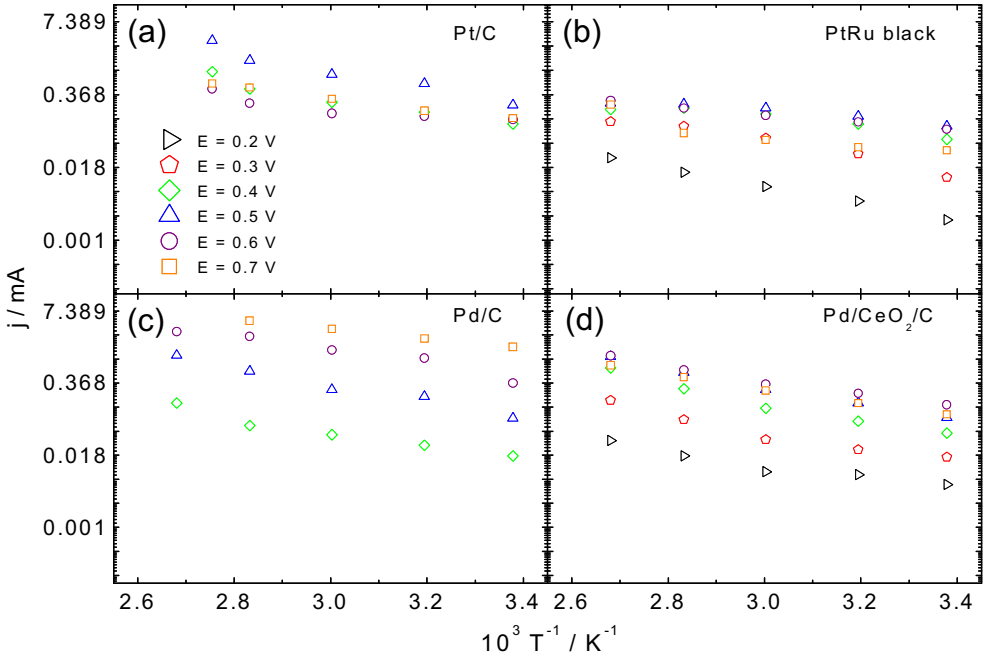

Fig. 6. Arrhenius plots of the steady-state ethanol oxidation current in 0.1 M ethanol + 0.5 M NaOH solution at different potentials (values see figure, data see Fig. 4) on different catalyst electrodes: (a) Pt/C (after 15 min), (b) PtRu black, (c) Pd/C, and (d) Pd/CeO_2/C. Electrolyte flow rate 15 μl s^{-1}, Faradaic currents measured after about 300 s, if not mentioned otherwise.

conditions, C–C bond rupture becomes rate limiting, and the resulting E_a should correspond to the activation barrier for this step at 0.7 V.

Similar trends for the activation energy were reported also for methanol oxidation on Pt/C catalysts in alkaline electrolyte. Cohen et al. [63] determined apparent activation energies for methanol oxidation on polycrystalline Pt electrode in the range between 16 and 39 kJ mol^{-1}, depending on the reaction potential. These data were obtained from the anodic sweep data in potentiodynamic measurement in 0.1 M KOH containing 0.5 M methanol solution. They found the apparent activation energies to first decrease with potential, reaching a minimum value at about 0.8 V_{RHE} (−0.125 V vs. Ag/AgCl) and then increase again with higher potentials, where oxide formation replaces OH^- adsorption [63].

For reaction on PtRu black, the higher coverages of OH_{ad} species on Ru sites improves the oxidative removal of dissociated adsorbate species, although the differences are less pronounced than in acidic electrolyte, and this way also promotes the incomplete oxidation of ethanol/acetaldehyde to acetate at the lower potential of 0.2 and 0.3 V. Since no C–C bond splitting is required for the incomplete oxidation reaction, the apparent activation energies are expected to change to lower values at lower potentials than on Pt/C, which agrees with the estimated values (Table 2).

For the Pd/C catalyst electrodes, E_a first increases with potential, from 24 ± 3 kJ mol^{-1} at 0.4 V to 29 ± 3 kJ mol^{-1} at 0.5 V, and then decreases to 24 ± 3 kJ mol^{-1} at 0.6 V and 17 ± 1 kJ mol^{-1} at 0.7 V. Finally, for the Pd/CeO_2/C catalyst, the tendency of the E_a values is comparable to that of the PtRu black catalyst, with E_a first being high, with 28 ± 4 kJ mol^{-1} at 0.3 V and 32 ± 3 kJ mol^{-1} at 0.4 V, and then decreasing to 24 ± 1 kJ mol^{-1} at 0.7 V (see Table 2). The lower value at 0.2 V for the Pd/CeO_2/C catalyst as compared to the PtRu black catalyst (30 ± 1 kJ mol^{-1}) may be rationalized by a facile supply of oxygen species by CeO_2 with its high capacity for storing/releasing oxygen or by an easier formation of oxygen-containing species on ceria, comparable to the role of Ru in PtRu, which improves the oxidation of adsorbed species accumulating on the Pd catalyst at low potentials [27,30,31,33,40,60,82,83].

The increase of E_a with higher potential, to ∼30 kJ mol^{-1} at 0.5 V, is likely to increasingly reflect the characteristics of C–C bond rupture on Pd, which becomes rate limiting due to the sufficient supply of oxygen-containing species. At higher potentials, 0.6 and 0.7 V, oxide formation on the surface is expected to increase the tendency for incomplete oxidation of ethanol to acetate, as deduced from the EOR selectivity at this potential in acidic medium [52]. In that case, the apparent activation energies are hardly comparable to those obtained on Pt/C, due to the different surface conditions. Similar values were also reported by Wang et al. for the electrooxidation of methanol, ethanol and 1-propanol on a Pd electrode (1.0 M KOH solution containing 1.0 M ethanol) using linear sweep voltammetry (LSV), where they obtained a value of 26.3 kJ mol^{-1} for the apparent activation energy at about 0.65 V_{RHE} (temperature range of 10–50 °C) [84], which agrees well with our result at 0.6 V.

For practical applications, the lower values of the apparent activation energy (in the range of 11–32 kJ mol^{-1}) indicate, that the further increase in activity with temperature will only be slow, significantly slower than for reaction in acidic environment.

4. Conclusions

Potentiodynamic and potentiostatic measurements of the alkaline electrooxidation of ethanol on different Pt-based (Pt/C and PtRu black) and Pd-based (Pd/C and Pd/CeO_2/C) thin-film catalyst electrodes, performed at elevated temperatures up to 100 °C and elevated pressure and under well-defined reaction and transport conditions, led to the following conclusions:

1. The activities for ethanol electrooxidation, as given by the steady-state currents, increases significantly with increasing reaction temperature for the different electrodes investigated. Only for the Pt/C catalyst at 0.4 and 0.5 V, the steady-state Faradaic currents first decrease with increasing temperature from 23 to 80 °C, followed by an increase above 80 °C.
2. The addition of Ru to Pt as well as of CeO_2 to Pd/C shifts the onset of ethanol oxidation reaction to lower potentials, increasing reaction temperature further promotes the negative shift of the onset potentials to low values.
3. The difference in the ratio of peak currents in negative-going scans vs. positive-going scans between Pt-based catalyst (below 1) and Pd-based electrodes (above 1) points to distinct differences in the potential dependent coverages of adsorbate species and in the influence of these adsorbed species on the reaction process on the respective catalysts.
4. Comparing the mass specific and active surface area normalized activities for ethanol oxidation reaction on the respective electrodes at 80 °C and at 23 °C shows different characteristics: the highest mass specific and active surface area specific activities are obtained on the Pd/C catalyst at high potential of 0.7 V at both temperatures (23 and 80 °C); for the Pt/C catalyst, higher activities are obtained at 0.5 V (23 °C) and 0.7 V (80 °C), respectively. At more positive potentials, higher mass specific/active surface area specific activities are obtained on the monometallic catalyst (Pt/C > PtRu black and Pd/C > Pd/CeO_2/C).
5. The linear correlation between ln j and $1/T$ in the corresponding Arrhenius plots on Pt-based and Pd-based catalyst indicates that the rate limiting steps do not change in the entire reaction temperature range, with the possible exception of the Pt catalyst. They result in apparent activation energies in the range of 11–32 kJ mol^{-1}.

Finally, the distinct temperature effects in the alkaline ethanol electrooxidation reaction on different electrodes resolved in the present study once more emphasize the importance of fuel cell relevant reaction and mass transport conditions in model studies on fuel cell reactions.

Acknowledgments

This work was supported by the Federal Ministry of Research and Technology (project 03SF0311C) and by the Baden-Württemberg Foundation within the project 'Portable Mini-Fuel Cells' (grant No. MBZ 20). We thank Dr. L. Jörissen (ZSW Ulm, Germany) for providing us with the catalysts.

References

[1] B. Beden, M.C. Morin, F. Hahn, C. Lamy, J. Electroanal. Chem. 229 (1987) 353.
[2] T. Iwasita, E. Pastor, Electrochim. Acta 39 (1994) 531.
[3] S.-G. Sun, in: J. Lipkowski, P.N. Ross (Eds.), Electrocatalysis, Wiley-VCh, New York, 1998 (Chapter 6).
[4] C. Lamy, A. Lima, V. LeRhun, F. Delime, C. Coutanceau, J.-M. Léger, J. Power Sources 105 (2002) 283.
[5] C. Lamy, S. Rousseau, E.M. Belgsir, C. Coutanceau, J.-M. Léger, Electrochim. Acta 49 (2004) 3901.
[6] R. Dillon, S. Srinivasan, A.S. Arico, V. Antonucci, J. Power Sources 127 (2004) 112.
[7] F. Vigier, C. Coutanceau, A. Perrard, E.M. Belgsir, C. Lamy, J. Appl. Electrochem. 34 (2004) 439.
[8] E. Antolini, J. Power Sources 170 (2007) 1.
[9] V.S. Bagotzky, Y.B. Vassiliev, O.A. Khazova, J. Electroanal. Chem. 81 (1977) 229.
[10] E. Antolini, E.R. Gonzalez, J. Power Sources 195 (2010) 3431.
[11] J.R. Varcoe, R.C.T. Slade, Fuel Cells 5 (2005) 187.
[12] J.R. Varcoe, R.C.T. Slade, Electrochem. Commun. 8 (2006) 839.
[13] J.R. Varcoe, R.C.T. Slade, E. Lam How Yee, Chem. Commun. (2006) 1428.
[14] S. Gu, R. Cai, T. Luo, Z. Chen, M. Sun, Y. Liu, G. He, Y. Yan, Angew. Chem. Int. Ed. 48 (2009) 6499.
[15] T.S. Zhao, Y.S. Li, S.Y. Shen, Front. Energy Power Eng. China 4 (2010) 443.
[16] J.A. Caram, C. Gutierrez, J. Electroanal. Chem. 323 (1992) 213.

[17] V. Rao, C. Hariyanto, C. Cremers, U. Stimming, Fuel Cells 5 (2007) 417.
[18] C. Cremers, D. Bayer, B. Kintzel, M. Joos, F. Jung, M. Krausa, J. Tübke, ECS Trans. 16 (2008) 1263.
[19] S.C.S. Lai, M.T.M. Koper, Phys. Chem. Chem. Phys. 11 (2009) 10446.
[20] L. Jiang, A. Hsu, D. Chu, R. Chen, Int. J. Hydrogen Energy 35 (2010) 365.
[21] S.C.S. Lai, S.E.F. Kleijn, F.T.Z. Öztürk, V.C. van Rees Vellinga, J. Koning, P. Rodriguez, M.T.M. Koper, Catal. Today 154 (2010) 92.
[22] A. Santasalo-Aarnio, Y. Kwon, E. Ahlberg, K. Kontturi, T. Kallio, M.T.M. Koper, Electrochem. Commun. 13 (2011) 466.
[23] A.V. Tripkovic, K.Dj. Popovic, J.D. Lovic, Electrochim. Acta 46 (2001) 3163.
[24] W. Zhou, Z. Zhou, S. Song, W. Li, G. Sun, P. Tsiakaras, Q. Xin, Appl. Catal. B 46 (2003) 273.
[25] L.H. Jiang, G.-Q. Sun, Z. Zhou, W.-J. Zhou, X. Qin, Catal. Today 93–95 (2004) 665.
[26] A.O. Neto, R.R. Dias, M.M. Tusi, M. Linardi, E.V. Spinacé, J. Power Sources 166 (2007) 87.
[27] A.V. Tripkovic, K.D. Popovic, B.N. Grgur, B. Blizanac, P.N. Ross, N.M. Markovic, Electrochim. Acta 47 (2002) 3707.
[28] V. Rao, C. Cremers, U. Stimming, L. Cao, S. Sun, S. Yan, G. Sun, Q. Xin, J. Electrochem. Soc. 154 (2007) B1138.
[29] H. Wang, C. Xu, F. Cheng, S. Jiang, Electrochem. Commun. 9 (2007) 1212.
[30] C. Xu, L. Cheng, P. Shen, Y. Liu, Electrochem. Commun. 9 (2007) 997.
[31] C. Xu, P. Shen, Y. Liu, J. Power Sources 164 (2007) 527.
[32] C.W. Xu, H. Wang, P.K. Shen, S.P. Jiang, Adv. Mater. 19 (2007) 4256.
[33] C. Xu, Z. Tian, P. Shen, S. Jiang, Electrochim. Acta 53 (2008) 2610.
[34] Q. Shen, Q. Min, J. Shi, L. Jiang, J. Zhang, W. Hou, J. Zhu, J. Phys. Chem. C 113 (2009) 1267.
[35] C. Bianchini, P.K. Shen, Chem. Rev. 109 (2009) 4183.
[36] Z.X. Liang, T.S. Zhao, J.B. Xu, L.D. Zhu, Electrochim. Acta 54 (2009) 2203.
[37] X. Fang, L. Wang, P.K. Shen, G. Cui, C. Bianchini, J. Power Sources 195 (2010) 1375.
[38] S. Uhm, Y. Yi, J. Lee, Catal. Lett. 138 (2010) 46.
[39] H.T. Zheng, Y.L. Li, S.X. Chen, P.K. Shen, J. Power Sources 163 (2006) 371.
[40] P.K. Shen, C. Xu, Electrochem. Commun. 8 (2006) 184.
[41] J. Fuhrmann, H. Zhao, E. Holzbecher, H. Langmach, M. Chojak, R. Halseid, Z. Jusys, R.J. Behm, Phys. Chem. Chem. Phys. 10 (2008) 3784.
[42] T.J. Schmidt, H.A. Gasteiger, G.D. Stäb, P.M. Urban, D.M. Kolb, R.J. Behm, J. Electrochem. Soc. 145 (1998) 2354.
[43] M. Chojak Halseid, Z. Jusys, R.J. Behm, J. Phys. Chem. C 114 (2010) 22573.
[44] J.S. Spendelow, J.D. Goodpaster, P.J.A. Kenis, A. Wieckowski, J. Phys. Chem. B 110 (2006) 9545.
[45] G. Garc¡a, M.T.M. Koper, J. Am. Chem. Soc. 131 (2009) 5384.
[46] F. Maillard, S. Schreier, M. Hanzlik, E.R. Savinova, S. Weinkauf, U. Stimming, Phys. Chem. Chem. Phys. 7 (2005) 385.
[47] E.G. Ciapina, S.F. Santos, E.R. Gonzalez, J. Electroanal. Chem. 644 (2010) 132.
[48] E. Lee, A. Murthy, A. Manthiram, Electrochem. Commun. 13 (2011) 480.
[49] F.H.B. Lima, J.R.C. Salgado, E.R. Gonzalez, E. Ticanelli, E.A. Ticianelli, J. Electrochem. Soc. 154 (2007) A369.
[50] A. Czerwinski, J. Electroanal. Chem. 379 (1994) 487.
[51] M. Grden, Electrochim. Acta 54 (2009) 909.
[52] S. Sun, M. Chojak-Halseid, M. Heinen, Z. Jusys, R.J. Behm, J. Power Sources 190 (2009) 2.
[53] N.M. Markovic, T.J. Schmidt, B.N. Grgur, H.A. Gasteiger, R.J. Behm, P.N. Ross, J. Phys. Chem. B 103 (1999) 8568.
[54] D.M. Drazic, A.V. Tripkovic, K.D. Popovic, J.D. Lovic, J. Electroanal. Chem. 466 (1999) 155.
[55] T.J. Schmidt, P.N. Ross, N.M. Markovic, J. Phys. Chem. B 105 (2001) 12082.
[56] G. García, M.T.M. Koper, Phys. Chem. Chem. Phys. 10 (2008) 3802.
[57] G. García, M.T.M. Koper, Phys. Chem. Chem. Phys. 11 (2009) 11437.
[58] G. García, P. Rodriguez, V. Rosca, M.T.M. Koper, Langmuir 25 (2009) 13661.
[59] J.C. Davies, G. Tsotridis, J. Phys. Chem. C 112 (2008) 3392.
[60] N. Wakabayashi, H. Uchida, M. Watanabe, Electrochem. Solid State Lett. 5 (2002) E62.
[61] E. Herrero, B. Alvarez, J.M. Feliu, S. Blais, Z. Radovic-Hrapovic, G. Jerkiewicz, J. Electroanal. Chem. 567 (2004) 139.
[62] R.J. Behm, Z. Jusys, J. Power Sources 154 (2006) 327.
[63] J.L. Cohen, D.J. Volpe, H.D. Abruña, Phys. Chem. Chem. Phys. 9 (2007) 49.
[64] Q. Wang, G.Q. Sun, L.H. Jiang, Q. Xin, S.G. Sun, Y.X. Jiang, S.P. Chen, Z. Jusys, R.J. Behm, Phys. Chem. Chem. Phys. 9 (2007) 2686.
[65] A.V. Tripkovic, S. Strbac, K.Dj. Popovic, Electrochem. Commun. 5 (2003) 484.
[66] H.A. Gasteiger, N. Markovic, P.N. Ross, E.J. Cairns, J. Electrochem. Soc. 141 (1994) 1795.
[67] J. Kua, W.A. Goddard III, J. Am. Chem. Soc. 121 (1999) 10928.
[68] J. Melke, A. Schoekel, D. Dixon, C. Cremers, D.E. Ramaker, C. Roth, J. Phys. Chem. C 114 (2010) 5914.
[69] H. Wang, Z. Jusys, R.J. Behm, J. Power Sources 154 (2006) 351.
[70] J. Prabhuram, R. Manoharan, H.N. Vasan, J. Appl. Electrochem. 28 (1998) 935.
[71] M. Grden, J. Kotowski, A. Czerwinski, J. Solid State Electrochem. 4 (2000) 273.
[72] M. Grden, A. Czerwinski, J. Solid State Electrochem. 12 (2008) 375.
[73] A. Trovarelli, in: Catalysis by Ceria and Related Materials, Imperial College Press, London, 2002.
[74] J.S. Spendelow, J.D. Goodpaster, P.J.A. Kenis, A. Wieckowski, Langmuir 22 (2006) 10457.
[75] E.H. Yu, K. Scott, R.W. Reeve, Fuel Cells 3 (2003) 169.
[76] A.V. Tripkovic, K.Dj. Popovic, J.D. Momcilović, D.M. Drazic, J. Electroanal. Chem. 418 (1996) 9.
[77] J.P. Liu, J.Q. Ye, C.W. Xu, S.P. Jiang, Y.X. Tong, Electrochem. Commun. 9 (2007) 2334.
[78] M. Nie, H.L. Tang, Z.D. Wei, S.P. Jiang, P.K. Shen, Electrochem. Commun. 9 (2007) 2375.
[79] Z.Y. Zhou, Q. Wang, J.L. Lin, N. Tian, S.G. Sun, Electrochim. Acta 55 (2010) 7995.
[80] J. Datta, A. Dutta, S. Mukherjee, J. Phys. Chem. C 115 (2011) 15324.
[81] D. Bayer, C. Cremers, H. Baltruschat, J. Tübke, ECS Trans. 41 (2011) 1669.
[82] C. Xu, P. Shen, J. Power Sources 142 (2005) 27.
[83] H. Yuan, D. Guo, X. Li, L. Yuan, W. Zhu, L. Chen, X. Qiu, Fuel Cells 9 (2009) 121.
[84] D. Wang, J. Liu, Z. Wu, J. Zhang, Y. Su, Z. Liu, C. Xu, Int. J. Electrochem. Sci. 4 (2009) 1672.